PROCEEDINGS OF SCIENCE

Polarized ^{129}Xe for Medical Applications

F.William Hersman, PhD[1]
University of New Hampshire
Durham, NH, United States
E-mail: hersman@unh.edu

Jan H. Distelbrink, PhD
Xemed LLC
Durham, NH, United States
E-mail: jand@xemed.com

Jeffrey Ketel
Xemed LLC
Durham, NH, United States
E-mail: jketel@xemed.com

Stephen Ketel
Xemed LLC
Durham, NH, United States
E-mail: sketel@xemed.com

Steve Bryn
Xemed LLC
Durham, NH, United States
E-mail: sbryn@xemed.com

David W. Watt, PhD
Xemed LLC
Durham, NH, United States
E-mail: dwatt@xemed.com

Walter C. Porter, M.S.
Xemed LLC
Durham, NH, United States
E-mail: wporter@xemed.com

1 Speaker

PoS(PSTP 2013)063

PROCEEDINGS OF SCIENCE

Jaime F. Mata, PhD
University of Virginia
Charlottesville, VA, United States
E-mail: jfm4q@virginia.edu

Iulian C. Ruset, PhD
Xemed LLC
Durham, NH, United States
E-mail: icruset@xemed.com

We present a xenon-129 polarizing system capable of sustaining clinical research with multiple dose inhalations within a single imaging session. The concept of counterflow polarizing was scaled-up using a high-power spectrally-narrowed laser, a 16-channel copper column, and a high-volume cryo-accumulation system. We present a general description of the system with focus on the key components. Polarization values of 60% in the delivery dose Tedlar bags were observed. More than 500 liters of xenon have been polarized for human lung imaging experiments at a single imaging site.

XVth International Workshop on Polarized Sources, Targets, and Polarimetry
September 9-13, 2013
Charlottesville, Virginia, USA

PoS(PSTP 2013)063

1. Background

Hyperpolarized (HP) noble gases, especially xenon-129 (129Xe) and helium-3 (3He) have shown promise for use as contrast agents for magnetic resonance imaging (MRI) of pulmonary function [1][2]. Due to the limited supply of 3He and its singular importance to other applications [3], considerable attention is directed at improving production of HP 129Xe for medical imaging. 129Xe is hyperpolarized using spin-exchange optical pumping (SEOP) [4]. The SEOP process requires a laser tuned to the wavelength that matches the D1 absorption line of an alkali metal, such as rubidium (Rb). The laser beam propagates along the axis of a magnetic field and illuminates a gas mixture comprised of the xenon gas to be polarized, the Rb vapor, a gas to quench photo-excited Rb (nitrogen), and tyically a buffer gas (helium-4). By exciting the Rb with angular momentum transfer, the circular polarization of the laser light depopulates Rb ground state levels with opposing spin leaving only one spin orientation which will become the polarized state. Because atomic interactions between Rb and other atoms (especially xenon) depolarize the Rb, the laser must continually replenish the Rb polarized state. When a polarized Rb atom collides with a 129Xe atom there is a probability that the nuclear spin of the 129Xe atom will acquire the orientation of the Rb electron polarization in a process called spin-exchange. The probability of spin-exchange is significantly increased if the Rb-Xe collision forms a longer-lived van der Waals molecule, which dominates the spin-exchange rate in the low pressure regime [5]. Over extended exposure times, the Xe polarization will asymptotically equilibrate toward the polarization of the Rb atoms.

The design of the high-throughput clinical xenon polarizer prototype presented here is based on the original counterflow polarizer [6][7]. There are three distinct functional regions: a Rb pre-saturator helix, a hot polarizing region, and a gas cooling and Rb condensation region (Fig. 1.) The Rb pre-saturator helix and the polarizing region in the lower part of the polarizing column are immersed in a silicone oil bath heated to an operating temperature of 140º-160ºC. The gas mixture of xenon, nitrogen, and helium enters the system through the glass helix and flows downward through the helix preloaded with puddles of Rb metal. As the gas temperature approaches the oil bath temperature it also saturates with Rb vapor. Upon entering the main polarizing column at its base, it flows upwards towards the polarizing laser light which enters the column through the top window. The spatial distribution of the Rb polarization in the polarizer depends on the local D1 laser intensity (optical pumping rate) and local spin destruction rate. During operation the Rb acquires a stable spatial distribution of its polarization along the column with the highest polarization closest to the laser and lower Rb polarization farther away. The xenon atoms from the gas mixture will start building up polarization as they flow through the polarized Rb, achieving their highest

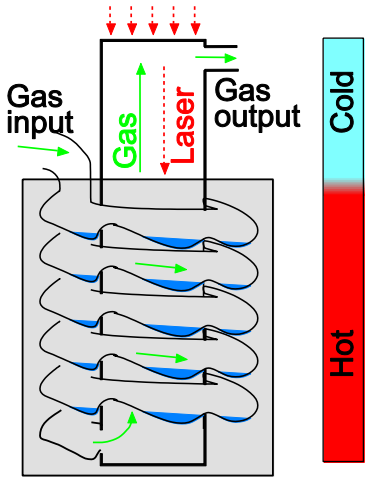

Fig.1: Concept of the counterflow polarizer showing the three operational regions: Rb vapor saturating helix (containing Rb puddles), spin-exchange optical pumping heated region, and Rb vapor deposition region.

polarization at the top of the hot zone. The cold zone is designed to extract the Rb vapor from the gas stream before it exits the laser illumination area. In the absence of the laser illumination Rb atoms depolarize within milliseconds and start to destroy the xenon polarization. The counterflow design provides continuous optical pumping of the Rb until it condenses. A powerful laser system would keep Rb polarization at its highest across the whole volume of the cell. However, if the laser is underpowered then the polarization of Rb will be distributed with its highest polarization closest to the hot-cold transition region where the laser enters the hot polarization region. Counterflow design is advantageous because the laser entrance coincides with the gas mixture exit, thus maximizing the accumulated xenon polarization as the gas flows through the system.

2.Materials & Methods

Advances in laser technology over the past several decades have enabled commensurate improvements in optical pumping. During the 1980s and early 1990s optical pumping was performed by increasingly capable technologies: resonance lamps, dye lasers, and then argon-ion pumped titanium-sapphire lasers. By the mid 1990s the optical pumping communinity transitioned to solid-state diode lasers whose lower cost and higher power efficiency made them well-suited for higher power applications. The large bandwidth of their wavelength output prevented all the light from being utilized. Resonant absorption of optical pumping light depends upon the pressure-broadened linewidth of the absorbing atoms. With absorption linewidths of approximately 0.06 nm for one atomsphere gas pressure, only a small fraction of the light from diode arrays with production linewidths of 2 nm to 4 nm would contribute to optical pumping. In fact, it was preffered to trade-off operating in the high pressure regime in order to maximize laser absorption, although there is a lower spin-exchange rate associated with it.

Within the last decade technology for narrowing the output of a diode array bar using wavelength-sensitive elements has been demonstrated. Chann et al. [8] used an afocal telescope to image optical rays onto an angled grating in the Littrow configuration, which then diffracted back to the laser cavity the selected wavelength for amplification. This approach has been used to achieve linewidths as small as 11 GHz (24pm) for a single diode array bar.

We sought methods to scale up the power output by narrowing a full stack of diode array bars [9]. The transverse dimension of a laser bar stack presented an impediment. An afocal telescope images a spatially extended light source in a plane perpendicular to the optical axis, however the grating is inclined at the Littrow angle. Bars displaced from the optical axis would be out of focus, preventing their light from being perfectly reimaged back on their emitters. The key improvement of our laser system (Fig. 2) is a step-mirror system within the locking cavity. The main purpose for the step-mirror

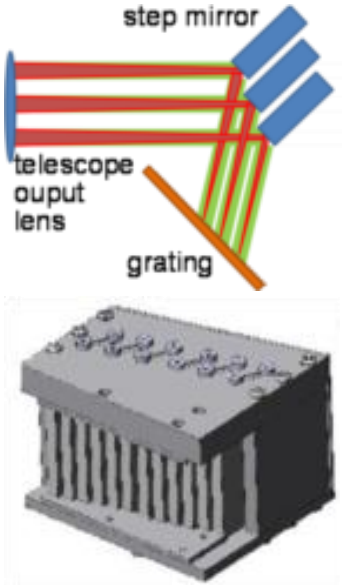

Fig. 2: a) schematic of the step mirror adjusting the optical path lengths (fast axis shown in green, slow axis in red); b) Step mirror assembly corresponding to a 12-bar array.

is to adjust the optical path for each laser bar such that all light rays come into perfect focus on the grating. Another important feature of the step-mirror is that it reduces the amount of the dark space between the emitting diode bars. The step-mirror and feedback grating are mounted together on a motorized rotational stage which provides final adjustment of the overall wavelength for the narrowed laser beam.

A more recent innovation corrects for the "smile" of the diode bars. Manufacturing imperfections in the flatness of the diode bars, so called "smile", is transformed into angle variations after the fast-axis microlens, and dominate the overall linewidth of the wavelength-locked laser output [8]. In order to remove this remaining variation, we characterized residual imperfections emitter-by-emitter in the output of each laser bar stack following a prescription by McBride [10]. Two parameters were measured: angular deflections caused by laser bar "smile" and greater-than-optimal divergence due to microlens distance variations. A correction plate with a corresponding array of curved prisms was fabricated consisting of unique correction elements for each emitter (PowerPhotonic, Fife, UK). This correction plate was permanently attached 2 mm in front of the laser stack and with excellent results (Fig. 3).

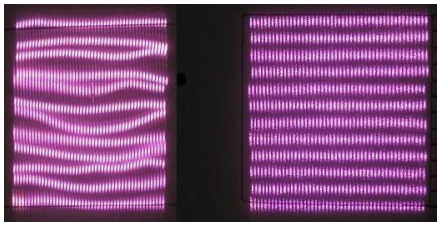

Fig. 3: Reduction of "smiles" for one 12-bar stack, shown before and after implementing a set of correction plates in front of factory microlenses.

These innovations are implemented in a system with 24 laser bars each capable of 100 watts free-running output. In our spectral narrowing system we de-rate the power output to 1.4 kW. The laser spectrum is shifted by adjusting the angle of the feedback grating in order to maximize its absorption by the Rb vapor. We obtained spectral resolution as narrow as 0.2 nm for each bar, with overall width of 0.3 nm

In order to dissipate the heat from this 1.4 kW laser, stabilize the temperature of the spin-exchange process [11], and scale-up the flow, we replaced the single glass column of the first demonstrated unit [6] with a 14x14 cm^2 square copper column augmented with internal copper fins (Fig. 4a). This geometry creates sixteen individual flow channels with copper walls that transfer the heat deposited by the laser into the surrounding oil bath. Additionally, the internal fins (Fig. 4b) give structural support such that the column can withstand low pressures. Concomitantly, this geometry is a good match for the low divergence laser beam whose shape is given by the stacked CW laser diode arrays. The top and bottom of the column were made as viewport flanges in order to accommodate fused silica windows for laser transparency. Insertion of a glass plate between the top (cold) and the bottom (hot) sections creates a thermal barrier in the column. The the one-meter long hot section and the half meter long cold section are precision-machined from oxygen-free copper and brazed together (Accurate Brazing, Goffstown, NH) using lead-free Cu-Ag brazing solder for thermal conductivity with the external walls. (Fig. 4c)

We report here a freeze-thaw xenon accumulation subsystem that is adapted and upgraded from our previously reported design [6]. By measuring the trapping fraction achieved by different glassware geometries, we determined that helical configurations offer the highest efficiency. Painting of xenon ice uniformly over the internal surface of the tubes by controllably raising the liquid nitrogen level over the time of the accumulation process increases the volume of xenon that can be efficiently recovered without clogging. The glassware was scaled-up to an eight-helix

component, where the input of the gas mixture splits to four glass helixes (Fig. 5b) immersed in a motorized liquid nitrogen (LN2) dewar system which is fully filled by an automated LN2 level controlling system. The dewar rises slowly in time and its motion is computer controlled via a LabVIEW interface and a stepper motor controller system. At the end of the accumulation process the LN2 dewar is lowered and replaced by a warm water container which, when in contact with the helix tubes, results in a quick thawing of the xenon back into the gas phase and dispensed into the Tedlar bags.

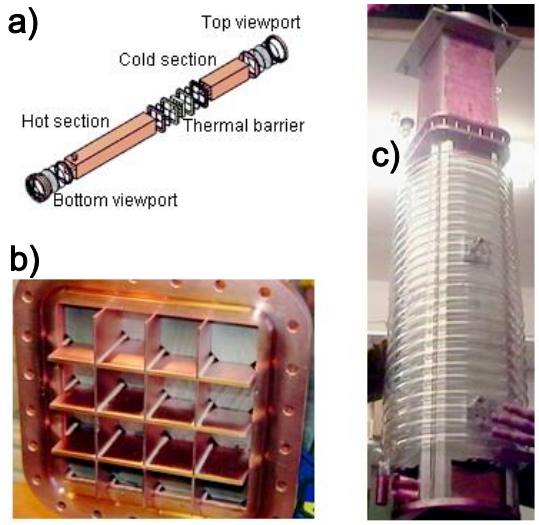

Fig.4: Copper polarizing column: a) Schematic showing subcomponents; b) Top side of the hot section during assembly. Sixteen individual channels are separated by copper fins. Temporary graphite spacers provide structural support during brazing; c) Final assembly includes the glass helix containing the Rb puddles for vapor saturation. The helix is being connected to the main body of the column at the base.

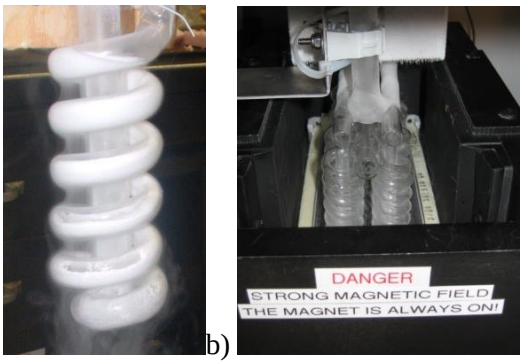

Fig. 5: a) Helical cryotrap showing a thin layer of xenon ice deposited on the inner surface. b) The cryogenic accumulating system is made of eight helical glass tubes which are gradually immersed in a rising LN2 dewar, such that the xenon is uniformily distributed along the length of the tubes. High magnetic field (~0.3T) provided by permanent magnet plates is needed for preserving polarization during phase transition changes.

3. Results & Discussion

Copper or metals are not commonly used as "wetted" materials for SEOP systems because of the shortened noble gas surface relaxation times on the order of minutes. We had estimated that the high spin-exchange rates available in the low pressure operating regime would be sufficient to overwhelm the shortened T_1 of xenon on copper. Optimal conditions are achieved not only with low overall pressure, but also with low xenon concentrations and high flow velocity.

The prototype polarizer was assembled as a partially-automated portable platform (Fig. 6a) to provide on-site HP 129Xe to clinical research partners. For the imaging experiments, two-liter batches were typically prepared each hour, with polarizing time of 20 minutes. The xenon flow rate through the system was 6 standard liter per hour. Polarizing parameters were: total pressure of 500 torr, nitrogen flow rate of 2 standard liter per minute (slm), helium flow rate of 6 slm, oil bath temperature 145ºC, laser operating current of 60 amperes corresponding to an output power of approximately 720W of narrowed spectrum. Following the thaw, the HP xenon is dispensed into as many as four Tedlar bags for inhalation. (Fig. 6b).

a)  b) 

Fig.6: a) Xenon polarizer in its compact portable enclosure shown next to the first author. b) Xenon batch dispensend in a combination of four dosing bags. The bags are attached to the connecting ports inside the polarizer niche.

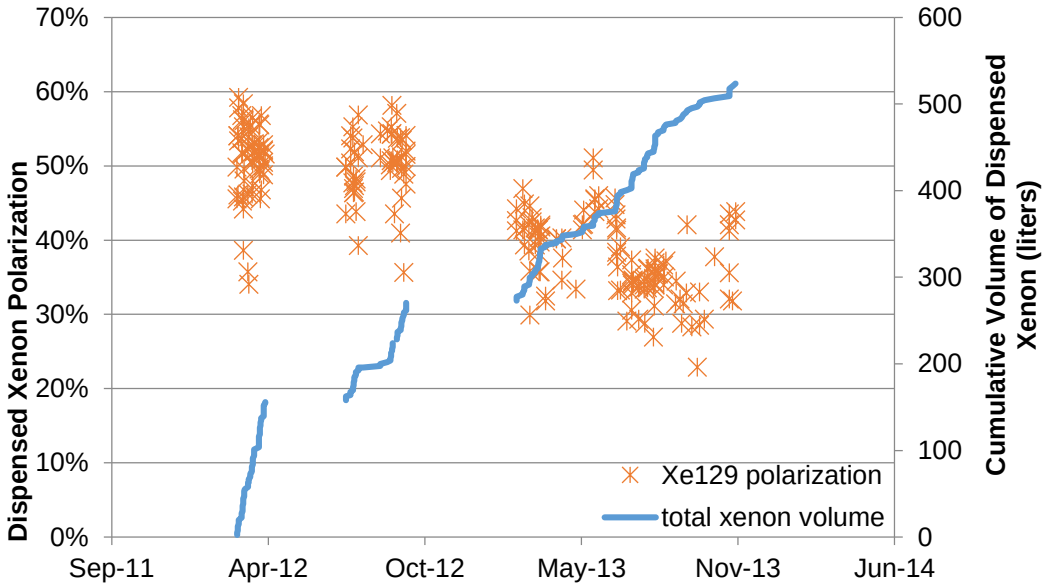

Fig.7 Xenon polarizations measured inside the Tedlar bags with a third-part NMR spectrometer range from 45% to 60%. An overall produced volume of 260 liters was delivered during 2012. In 2013 age-related partial laser bar failure lowered polarizations to ~28% to 45%.

For example, during a four month time period, this system delivered 600 bags of HP xenon which were used in 64 human subjects for MRI research studies. Most of these studies occurred at the University of Virginia as part of collaborative research to demonstrate safety and efficacy. All the human experiments were conducted under informed consent, following locally approved IRB protocols and Investigational New Drug protocols approved by the FDA to the University of New Hampshire and Xemed LLC. We imaged healthy subjects and patients with lung diseases including COPD, asthma, cystic fibrosis, and sickle cell disease. There were no reports of serious

adverse events related to HP xenon inhalation. The subjects inhaled up to one liter of HP xenon, usually supplemented with oxygen to maintain its concentration at the atmospheric level. Comparisons of ventilation anomalies between HP 129Xe lung ventilation images and comparable images acquired with HP 3He at two sites revealed that images with xenon were better at conspicuously delineating ventilation defects [2][12]. The high polarization and production rate from this prototype 129Xe polarizer and enabled novel imaging protocols that focused on xenon solubility in tissue and blood, and that are not possible with 3He [13][14].

In conclusion, we report technical developments that have enabled scale-up of production of HP 129Xe achieving polarizations in the 50% range at rates of several liters per hour. A prototype polarizer implementing these developments has been installed at several sites performing clinical research. Collaborative studies are ongoing using this polarizer to demonstrate safety and efficicacy for a range of diagnostic applications.

References

[1] S. Fain, M.L. Schiebler, D.G. McCormack, G. Parraga, *Imaging of lung function using hyperpolarized helium-3 magnetic resonance imaging: review of current and emerging translational methods and applications*, J.Magn.Reson.Imag. **32** (2010) 1398-1408.

[2] J.P. Mugler III, T.A. Altes, *Hyperpolarized ^{129}Xe MRI of the Human Lung*, J.Magn.Reson.Imag. **37** (2013) 313-331.

[3] A. Cho, Helium-3 shortage could put freeze on low-temperature research, Science **326** (2009) 778-779.

[4] T.G. Walker, W. Happer, *Spin-exchange optical pumping of noble-gas nuclei*, Rev.Mod.Phys. **69** (1997) 629-642.

[5] W. Happer, E. Miron, S. Schaefer, D. Schreiber, W.A. van Wijngaarden. Polarization of the nuclear spins of noble-gas atoms by spin-exchange with optically pumped alkali-metal atoms, Phys.Rev.A **29** (1984) 3092-3110.

[6] I.C. Ruset, S. Ketel, F.W. Hersman, Optical Pumping System Design for Large Production of Hyperpolarized ^{129}Xe, Phys.Rev.Lett. **96** (2006) 053002.

[7] F.W. Hersman, I.C. Ruset, S. Ketel, et al. Large Production System for Hyperpolarized ^{129}Xe for Human Lung Imaging Studies. Acad.Radiol. **15** (2008) 683-692.

[8] B. Chann, I. Nelson, T.G. Walker, *Frequency-narrowed external-cavity diode-laser-array bar*, Opt.Lett. **25** (2000) 1352-1354.

[9] H. Zhu, I.C. Ruset, F.W. Hersman, *Spectrally narrowed external-cavity high-power stack of laser diode array*, Opt.Lett. **30** (2005) 1342-1344.

[10] R. McBride, H. Baker, J.-L. Neron, et al. *A high brightness QCW pump source using a pre-aligned GRIN lens array with refractive beam correction*, Proc. of SPIE (2008) 6876.

[11] D.K. Walter, W.N. Griffith, W. Happer, *Energy transport in high-density spin-exchange optical pumping cells*, Phys Rev Lett. **86** (2001) 3264-3267.

[12] M. Kirby, S. Svenningsen, N. Kanhere, et al. *Pulmonary ventilation visualized using hyperpolarized helium-3 and xenon-129 magnetic resonance imaging: differences in COPD and relationship to emphysema* **114** (2013) 707-715.

[13] I. Dregely, J.P. Mugler III, I.C. Ruset, et al. *Hyperpolarized Xenon-129 gas-exchange imaging of lung microstructure: first case studies in subjects with obstructive lung disease* **33** (2011) 1052-1062.

[14] K. Qing, K. Ruppert, Y. Jiang, et al. *Regional mapping of gas uptake by red blood cells and tissue in the human lung using hyperpolarized xenon-129 MRI* DOI: 10.1002 (2013) jmri.24181.